PERGAMON

Journal of Structural Geology 23 (2001) 315–327

JOURNAL OF STRUCTURAL GEOLOGY

www.elsevier.nl/locate/jstrugeo

Faulted joints: kinematics, displacement–length scaling relations and criteria for their identification

Scott J. Wilkins[a,*], Michael R. Gross[a], Michael Wacker[a], Yehuda Eyal[b], Terry Engelder[c]

[a]*Department of Geology, Florida International University, Miami, FL 33199, USA*
[b]*Department of Geology, Ben Gurion University, Beer Sheva 84105, Israel*
[c]*Department of Geosciences, The Pennsylvania State University, University Park, PA 16802, USA*

Received 6 December 1999; accepted 6 June 2000

Abstract

Structural geometries and kinematics based on two sets of joints, pinnate joints and fault striations, reveal that some mesoscale faults at Split Mountain, Utah, originated as joints. Unlike many other types of faults, displacements (D) across faulted joints do not scale with lengths (L) and therefore do not adhere to published fault scaling laws. Rather, fault size corresponds initially to original joint length, which in turn is controlled by bed thickness for bed-confined joints. Although faulted joints will grow in length with increasing slip, the total change in length is negligible compared to the original length, leading to an independence of D from L during early stages of joint reactivation. Therefore, attempts to predict fault length, gouge thickness, or hydrologic properties based solely upon D–L scaling laws could yield misleading results for faulted joints. Pinnate joints, distinguishable from wing cracks, developed within the dilational quadrants along faulted joints and help to constrain the kinematics of joint reactivation.

1. Introduction

Brittle faults are distinguished mainly by slip parallel to the fracture plane. Despite this common property, faults can develop by one of several mechanisms depending on scale. A fault that defines a planar zone on a large scale is likely to have developed either through the coalescence of microcracks, joints, or opening-mode veins (e.g. Hancock, 1972; Beach, 1975; Ramsay and Huber, 1987; Willemse et al., 1997; Mollema and Antonellini, 1999), or through the linkage of smaller fault segments (e.g. Peacock, 1991; Peacock and Sanderson, 1991; Cartwright et al., 1995; Dawers and Anders, 1995; Willemse, 1997). However, another type of fault develops neither by linkage of cracks on a microscopic scale nor by linkage of small faults or joints on a mesoscopic scale. In this latter case, fracture-parallel slip is driven by a shear traction on a planar discontinuity, most likely a joint, that will subsequently develop a gouge or other structures of mechanical wear that are so common of typical faults. This contribution examines the impact of these "faulted joints" on displacement–length scaling relations and fault-slip kinematics.

Angelier (1994) differentiates between two types of isolated faults (i.e., faults without linked fault segments) at the mesoscale: "neoformed faults" which form and slip within the same stress field, and "inherited faults" which are pre-existing planes of weakness that slip within a stress regime different from the stress regime that existed during their formation. Due to confusion that may arise from using the term "neoformed", throughout this paper we refer to faults that initiate and slip within the same stress field as primary faults. Primary faults develop within a causative stress field leading to a resolved shear traction along the fault plane (Fig. 1a). Primary faults are sometimes found as conjugate pairs aligned such that the maximum principal stress (σ_1) falls within the plane of the acute bisector (Anderson, 1951; Hancock, 1985; Angelier, 1994). A combination of field (e.g. Hancock, 1972; Beach, 1975; Willemse et al., 1997; Mollema and Antonellini, 1999) and laboratory (Scholz, 1968; Lockner et al., 1992) studies demonstrate that primary faults initiate and grow through the coalescence and linkage of échelon extension fractures and microcracks. Consequently, a primary fault occupies a zone of deformation that may consist of varying amounts of breccia, gouge, and fractured rock created by a combination of fracture coalescence and shear strain during fault growth.

* Corresponding author. Present address: Department of Geology, Geomechanics–Rock Fracture Group, Mackay School of Mines/172, University of Nevada/Reno, Reno, NV 89557-0138, USA. Tel.: 00-1-775-784-6050; fax: 00-1-775-784-1833.

E-mail address: swilki@unr.edu (S.J. Wilkins).

0191-8141/01/$ - see front matter
PII: S0191-8141(00)00098-5

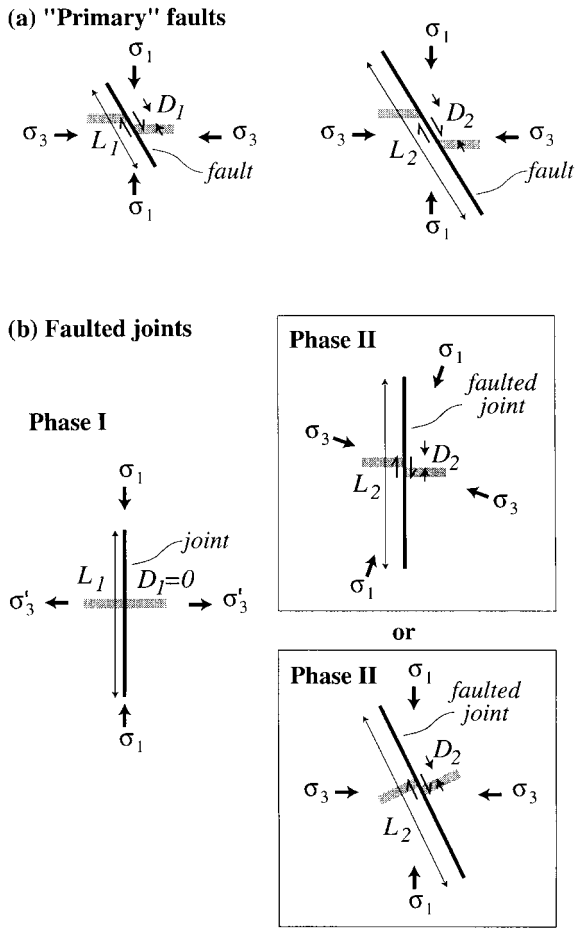

Fig. 1. Differences between primary faults and faulted joints. (A) Primary faults propagate and slip within the same stress field, often resulting in a systematic increase in displacement (D) with increasing fault length (L). (B) Faulted joints initiate as opening-mode fractures with zero shear displacement (Phase I). Slip occurs due to a realignment of the joint with respect to the surrounding stress field (Phase II), either due to a rotation of the stress field (top) or to the rotation of the joint within a fixed stress field (bottom). Note that faulted joints attain considerable length (L_1) prior to slip (D_2).

Joints are opening-mode fractures that propagate normal to the least principal stress (σ_3) and in the plane containing σ_1 and σ_2 (Fig. 1b). On the mesoscale, joints occur as either isolated single fracture planes or multiple fracture planes in the form of a joint zone (e.g. Bahat, 1988; Helgeson and Aydin, 1991). Due to the absence of slip, fault breccia or other cataclastic materials are not associated with joint formation. "Faulted joints" are a subclass of inherited faults that originate as mesoscale joints (e.g. Segall and Pollard, 1983; Cruikshank et al., 1991; Angelier, 1994). The generation of faulted joints involves two states of stress (Fig. 1b). The initial state is responsible for the generation of the joint set, during which the principal stresses are orthogonal and parallel to the joint set. Subsequently, faulted joints occur as a consequence of the misalignment of the principal stresses with respect to the joint plane so that the joint is subject to a shear traction. This misalignment leads to slip along the pre-existing joint, hence the term "reactivation" applies to faulted joints. Misalignment of the stress field can occur by two processes. First, the regional stress field can change orientation over time, as was the case for the Alleghanian stress field driving Appalachian Plateau tectonics (Younes and Engelder, 1999). Second, jointed beds can rotate within a regional stress field that remains fixed in orientation. This latter process leads to the faulted joints that we describe in this paper (Fig. 1b).

Shear displacement across faulted joints is accommodated by frictional sliding along a pre-existing plane of weakness (i.e. joint) rather than the propagation of new fault surface area. In the laboratory, this behavior leads to a lesser degree of gouge and breccia development than for primary faults that have experienced the same amount of displacement (Engelder et al., 1975). Consequently, although primary faults and faulted joints both display shear offset, their physical characteristics may differ markedly. Differences in fault zone architecture and geometry, in turn, will have a major impact on fluid flow within fractured and faulted bedrock (e.g. Marone and Scholz, 1989; Caine et al., 1996; Evans et al., 1997; Zhang and Tullis, 1998).

The difference between primary faults and faulted joints may also have implications for fault-scaling relations that are used to predict fault dimensions beyond the scale of observation (Childs et al., 1990), construct models for fault growth (Walsh and Watterson, 1988; Cowie and Scholz, 1992a), and estimate strain (Marrett and Allmendinger, 1992). Compilations of fault dimension data suggest that, as a general rule, the amount of slip on a fault is roughly proportional to its length (e.g. Walsh and Watterson, 1988; Cowie and Scholz, 1992b; Schlische et al., 1996). Although this rule may hold true for primary faults that develop in homogeneous media, one would not expect the same relationship for faults that originated as joints because a finite fracture length was achieved prior to shear displacement (Fig. 1b). In light of the importance of identifying faults that originated as joints, the goals of this contribution are to establish the kinematics and displacement–length scaling relations of faulted joints, and to present criteria for distinguishing faulted joints from primary faults. Although several studies have analyzed displacement–length (D–L) relations for large fault zones that utilized or incorporated extensional features (Opheim and Gudmundsson, 1989; Cartwright et al., 1995), to the best of our knowledge this study marks the first D–L analysis of isolated, mesoscale faulted joints.

2. Outcrop description

Field observations and data were collected from an outcrop on the southern limb of Split Mountain Anticline, an ~E–W-trending Laramide structure in northeast Utah (Fig. 2). The outcrop consists of interbedded sandstones, siltstones, and shales that dip 18° to the SSW, and contains the contact between the Chinle Formation and overlying

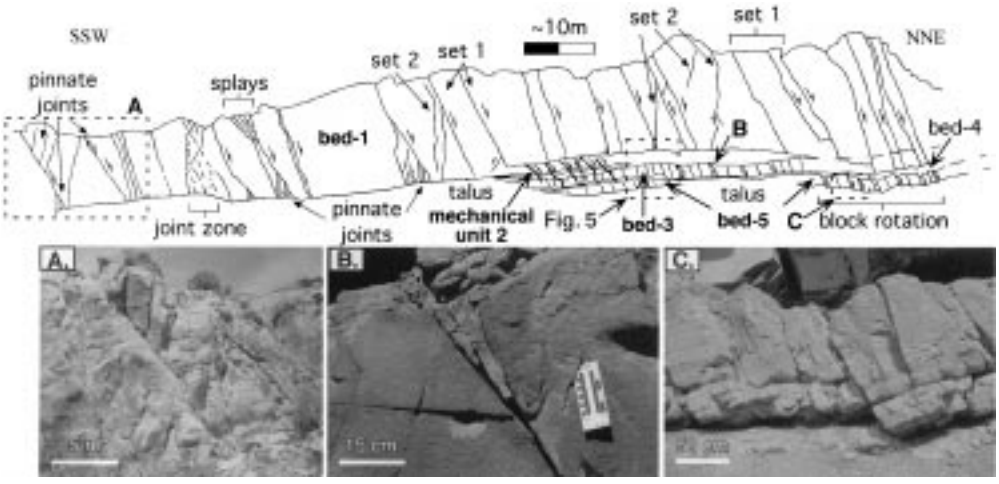

Fig. 2. Outcrop sketch from photomosaic of fractures exposed in a vertical section of interbedded sandstones and shales of the Glen Canyon Sandstone and Chinle Formation in the southern limb of Split Mountain Anticline, Utah (UTM 12, 4476140N, 653880W; Rowley and Hansen, 1979). Fractures are confined to individual beds and many N-dipping fractures display shear offset. (A) Photo of pinnate joints in the northern block of a large Set 1 faulted joint in Bed 1. (B) Photo of pinnate joints in the northern block of a Set 1 faulted joint in Bed 3. (C) Photo of rotated blocks along Set 1 faulted joints in Bed 5.

Glen Canyon Sandstone, which were deposited in the Late Triassic and Early Jurassic (Rowley and Hansen, 1979). Slip along reverse faults in the basement during the Early Tertiary folded the overlying sedimentary cover (Hansen, 1986). Regional shortening and folding led to the development of many brittle structures at the outcrop, including isolated and linked normal faults, bedding plane slip surfaces, and several joint sets (Silliphant, 1998; Wilkins, 1999).

Our study is restricted primarily to a kinematically linked group of joints and faulted joints confined to three prominent beds (hereafter referred to as jointed beds; refer to Fig. 3 for mechanical stratigraphy): a massive ~14-m-thick ridge-forming sandstone (Mechanical Unit 1), a ~1-m-thick sandstone (Mechanical Unit 3), and a ~1-m-thick silicified dolomitic siltstone (Mechanical Unit 5). In addition, we analyze isolated primary faults within a 1.2-m-thick lithologic sequence (Mechanical Unit 2) that is dominantly comprised of shale.

3. Description and analysis of joints and faults

3.1. Bed-confined joints

Fractures observed in Mechanical Units 1, 3 and 5 include two sets of bed-confined joints and associated smaller secondary fractures. The most pervasive fractures are Set 1 joints, aligned sub-normal to bedding with a mean orientation of 295° 62° N (strike, dip amount and direction; Fig. 4a). These joints are especially prominent in Bed 1, dividing the massive ridge-former into large joint-bounded blocks. Plumose structures are preserved on many Set 1 joint surfaces, implying pure opening-mode tip propagation. Most Set 1 joints span the entire bed thickness with joint tips residing at mechanical layer boundaries (Fig. 5). Joint spacing was measured as the perpendicular distance between adjacent Set 1 joints in the three jointed beds. Joint spacing histograms for each jointed bed, as well as a combined normalized spacing histogram for all beds, reveal positively skewed distributions (Fig. 6). Similar spacing distributions have been reported for mechanically confined joints in other layered sedimentary rocks (e.g. Narr and Suppe, 1991; Gross, 1993; Becker and Gross, 1996; Ji and Saruwatari, 1998; Ruf et al., 1998).

A less prominent set of joints (Set 2) is subvertical and strikes parallel to the Set 1 joints, with a mean orientation of 296° 83°N (Fig. 4c). Although mean dips of Set 1 and Set 2 joints are separated by only 21°, the two joint sets represent fracture populations whose mean orientations are statistically different from each other at the 95% confidence level. Although found in all three beds that contain Set 1 joints, Set 2 joints are more widely scattered throughout the outcrop and appear either as single fracture surfaces or as narrow zones of smaller, closely spaced joints. In contrast, Set 1 joints do not exhibit the morphology of fracture zones but rather always appear as single fracture surfaces. Most Set 2 joints terminate at mechanical layer boundaries, although a number of joints belonging to this set terminate within the jointed bed or against other joints. Where members of the two joint sets intersect, Set 2 joints always abut against, and hence post-date, Set 1 joints.

3.2. Faulted joints

Many Set 1 joints (48 of 171) in Beds 1, 3 and 5 display shear offset with downthrown northern hanging walls (Fig. 2). Interestingly, these fractures have little or no gouge and lack a conjugate fault set. Where present, striations on

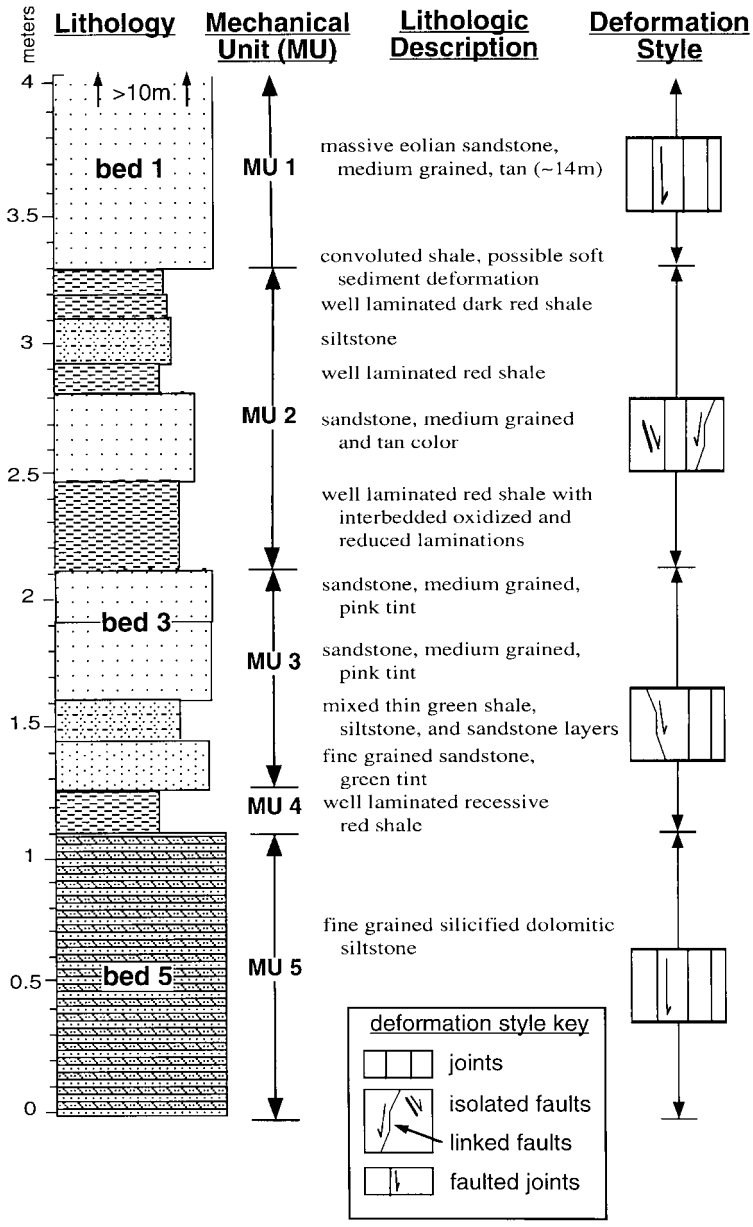

Fig. 3. Mechanical stratigraphy of the studied outcrop. The lower contact of the uppermost sandstone is interpreted as the contact between the Jurassic–Triassic Glen Canyon Sandstone (above) and the Triassic Chinli Formation (below).

these Set 1 surfaces are steeply plunging, indicating normal dip-slip fault movement (Fig. 4b). In Bed 5, slip along Set 1 joints resulted in a domino geometry due to localized block rotation (Fig. 2c). Slip along these Set 1 joints in Bed 5 dissipates into diffuse zones of minor folding and fracturing within the bounding shale beds, and there is no evidence for linkage of the slip surfaces with a sole fault. Confinement to jointed beds, lack of breccia/gouge and conjugates, and parallelism of joints and sheared fractures together imply that Set 1 fractures originated as joints, and that a significant number of those joints were subsequently reactivated in shear. We refer to this subset of Set 1 fractures as faulted joints.

3.3. Pinnate joints and wing cracks

Another group of fractures are pinnate joints, found in association with host Set 1 faulted joints (Fig. 2). Pinnate joints are relatively small, opening-mode fractures localized at acute angles along larger host faults (e.g. Hancock, 1985; Engelder, 1989). They have also been referred to as horsetail fractures (Cruikshank et al., 1991). Pinnate joints are found in clusters near the bottoms and tops of beds containing Set 1 joints. Where present near the bases of beds, the pinnate joints are located in the footwall beneath Set 1 faulted joints (Fig. 2). Pinnate joints near the tops of beds are found in the hanging wall above Set 1 faulted joints. The

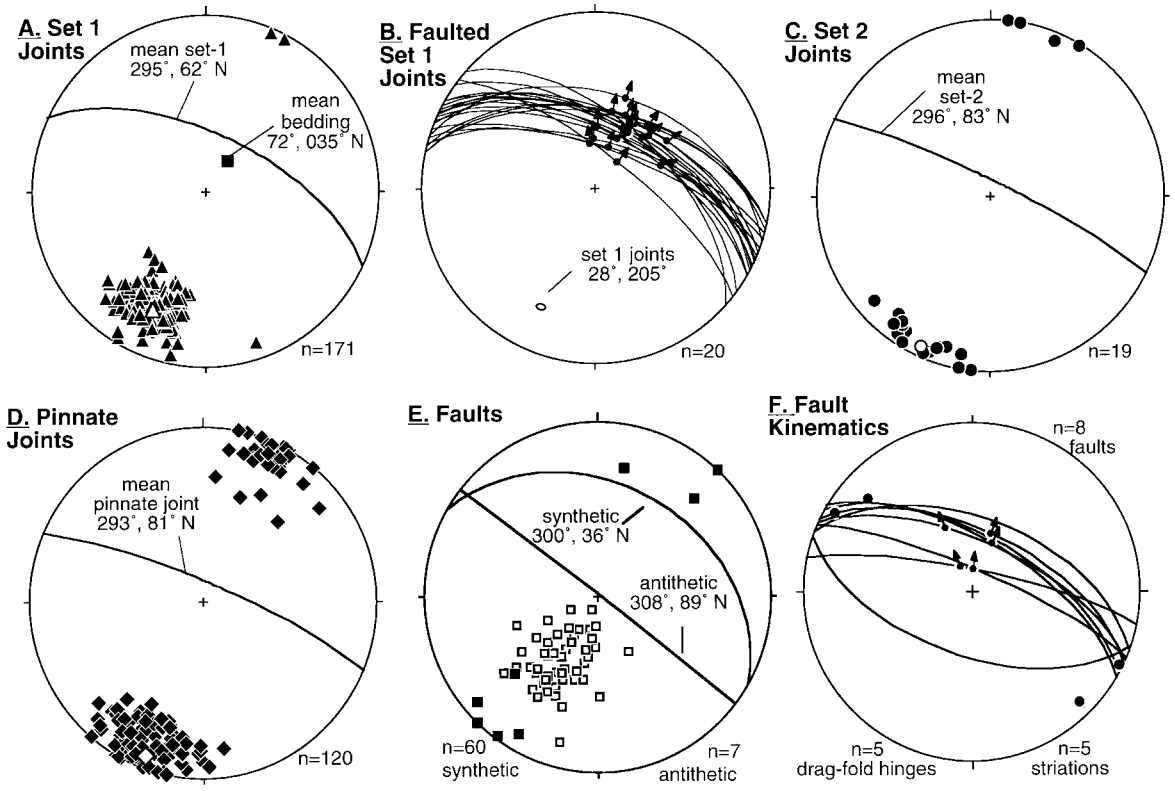

Fig. 4. Lower hemisphere equal-area projections of fracture orientations and related structures. (A) Poles to Set 1 joints in Beds 1, 3, and 5 (black triangles), and mean pole (white triangle). Mean pole to bedding is shown as a black square. (B) Orientations of faulted Set 1 joints (great circles) and their striations (black circles with arrows indicating motion of hanging wall). Small circle is 95% confidence area for Set 1 joints. (C) Poles to Set 2 joints in Bed 1 (black circles), and mean pole (white circle). (D) Poles to pinnate joints (black diamonds) found adjacent to Set 1 host fractures, and mean pole (white diamond). (E) Poles to conjugate primary faults (synthetic white squares, antithetic black squares). Great circles represent mean orientations of conjugate faults. (F) Orientations of primary faults (great circles) and associated kinematic indicators including striations (circles with arrows) and drag fold hinges (circles).

mean orientation of the pinnate joints is 293° 81°N (Fig. 4d), parallel to the Set 2 subvertical joints (Fig. 4c). The calculated angle between individual pinnate joints and their host fracture ranges between 4° and 44°, with an average of 19° (Fig. 7). Whereas the overwhelming majority of pinnate joints are found adjacent to slipped Set 1 joints, in some cases pinnate joints abut host fractures that lack measurable displacement.

Several prominent wing cracks were observed emanating from tips of unconfined Set 1 joints. The wing cracks curve to become parallel with Set 2 joints. Also referred to as splay cracks (Martel and Pollard, 1989; Cooke, 1997) or kinks (Cruikshank et al., 1991), wing cracks are opening-mode fractures oriented oblique to the host fracture, and may represent "out of plane" propagation (i.e. relative to Set 1 fractures) due to mixed mode or shear loading along the host fracture (Cotterell and Rice, 1980; Nemat-Nasser and Horii, 1982; Cruikshank et al., 1991; Willemse and Pollard, 1998). Unlike the planar pinnate joints that initiate along the length of the host fracture, wing cracks initiate from the host fracture tip and often curve dramatically over short distances to become aligned parallel to the remote compressive stress.

3.4. Primary faults

Isolated primary faults (hereafter referred to as primary faults) are found in shale beds within Mechanical Unit 2 (Fig. 3) and appear as two conjugate sets, although the faults are not equally distributed between the two sets. Primary faults belonging to the dominant conjugate set are synthetic to the faulted Set 1 joints, display downthrown northern blocks and are characterized by a mean orientation of 300° 36°N (Fig. 4e). The less abundant primary faults (antithetic to Set 1 faulted joints) have downthrown southern blocks and a mean orientation of 308° 89°N (Fig. 4e). Where present, the attitudes of striations on primary fault surfaces indicate dip-slip motion (Fig. 4f). Upon restoring bedding to horizontal, mean orientations for the synthetic and antithetic primary faults are 301° 54°N and 128° 73°S, respectively (Fig. 8a), remaining approximately parallel in strike to Set 1 and Set 2 joints (Fig. 4a, c).

3.5. Displacement–length relations for primary faults and faulted joints

Maximum dip separation and cross-sectional trace length were measured for faulted Set 1 joints and isolated primary

Fig. 5. Photo of bed-confined joints within Bed 1 (top), Bed 3 (middle), and Bed 5 (bottom). Arrows point to Set 1 joint tips at bed boundaries.

faults. In light of the observed dip-slip kinematics on both Set 1 faulted joints and primary faults (Fig. 4b, f), the dip separation (defined as the distance or separation of formerly adjacent beds on either side of a fault surface measured along the dip of the fault; Bates and Jackson, 1995) corresponds to the magnitude of displacement. Bedding surfaces and numerous alternating oxidized (red) and reduced (green) horizons served as excellent marker horizons to accurately measure the maximum displacement across the faults. Although the geological community has not adopted a standard geometric or kinematic nomenclature for defining fault dimensions, we follow the terminology of

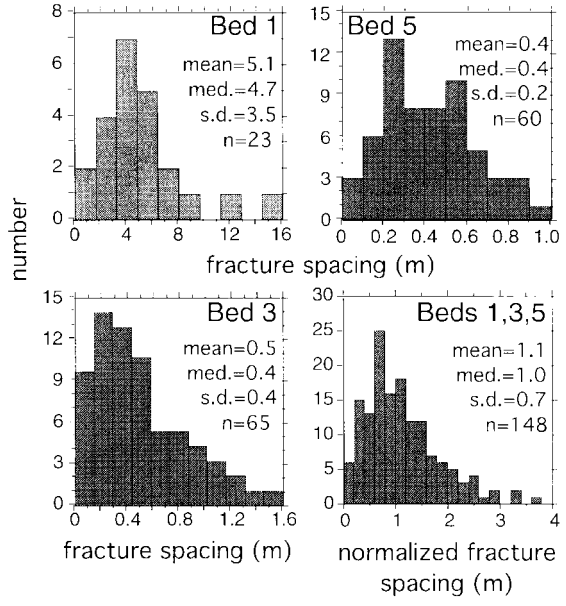

Fig. 6. Histograms of fracture spacing for Set 1 joints within Beds 1, 3, 5, and three beds combined with normalized data.

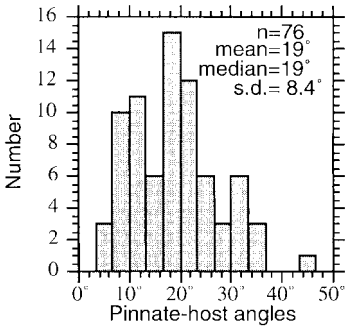

Fig. 7. Histogram of angle between individual pinnate joints and their host fractures.

Watterson (1986) and Walsh and Watterson (1988), who define fault length (L) as the dimension parallel to the slip vector and fault width (W) as the dimension normal to the slip vector. We further note that linear correlations between displacement and length have been established for normal faults both measured along strike (e.g. Walsh and Watterson, 1988; Dawers et al., 1993) and in cross-section (e.g. Muraoka and Kamata, 1983; Gross et al., 1997).

The resulting displacement–length plot reveals fundamental differences in scaling between faulted joints and primary faults at Split Mountain (Fig. 9). Primary faults within Mechanical Unit 2 display a general increase in fault displacement with length. The power-law curve fit ($D = 0.0058L^{1.19}$, $R^2 = 0.99$) is characterized by a high correlation coefficient and a power law exponent of $\sim$1, indicating that displacement across isolated primary faults correlates in an approximately linear fashion with fault length, similar to other data sets analyzed in the literature (e.g. Cowie and Scholz, 1992b; Clark and Cox, 1996; Schlische et al., 1996). The average D/L ratio for isolated primary faults is 0.013. In contrast to primary faults, lengths of faulted joints are relatively uniform within a given bed, reflecting their initiation as bed-confined joints whose dimensions are controlled by bed thickness. Note that for each bed the amount of displacement observed across faulted joints is independent of trace length, resulting in poor correlation coefficients (R^2 for power-law curve fits of 0.27, 0.08, and 0.04 for Beds 1, 3, and 5, respectively). When faults from each bed are grouped together, the average D/L ratios are 0.010, 0.014, and 0.04 for Beds 1, 3, and 5, respectively.

3.6. Kinematic and stress analysis of joints and primary faults

Our interpretation, that measured Set 1 slip surfaces are indeed faulted joints, must be consistent with the kinematic and structural history of the outcrop. Fortunately, fracture geometries, surface morphologies, orientations, dimensions, fault striations, and cross-cutting relations provide the necessary constraints for a kinematic and structural

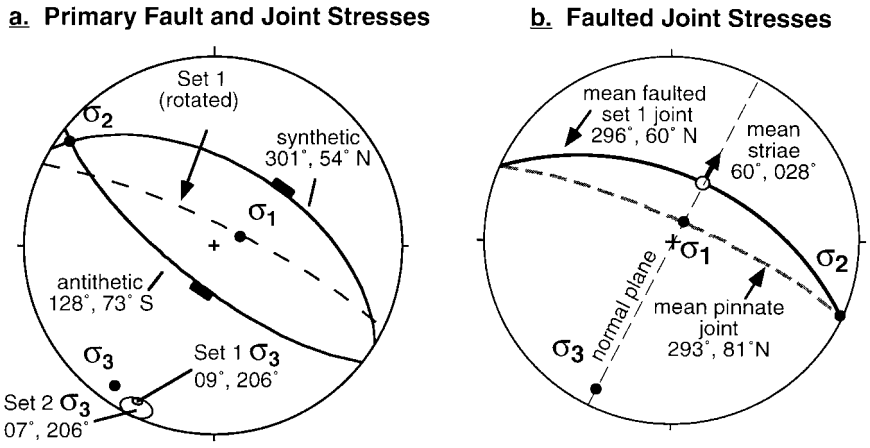

Fig. 8. (A) Principal stress axes derived from primary faults with bedding rotated to the horizontal. Note subvertical σ_1, and also subhorizontal σ_3, closely aligned to 95% confidence area of orientations for rotated Set 1 and Set 2 joints. (B) Principal stress axes derived from faulted Set 1 joints based on kinematic relations among pinnate joints, Set 2 joints, and striations on faulted Set 1 joints.

interpretation. In the following paragraphs we discuss the origin and kinematics of fractures in their interpreted order of formation: Set 1 joints and primary faults, followed by the coeval formation of Set 2 joints, pinnate joints, and slip along Set 1 joints. Subsequently, we utilize geometric relationships between pinnate joints and faulted joints to perform a type of paleostress analysis.

Abutting relations in the jointed beds indicate that Set 1 joints formed prior to Set 2 joints and pinnate joints. The small but significant difference in mean orientations between the two joint sets implies either a rotation of the stress field between joint set formation, or the passive rotation of beds carrying the earlier joint set within a fixed stress field. Because many of the observed fractures most likely developed during folding, we explore the possibility that the earlier joint set and primary faults may have rotated during tilting of the strata.

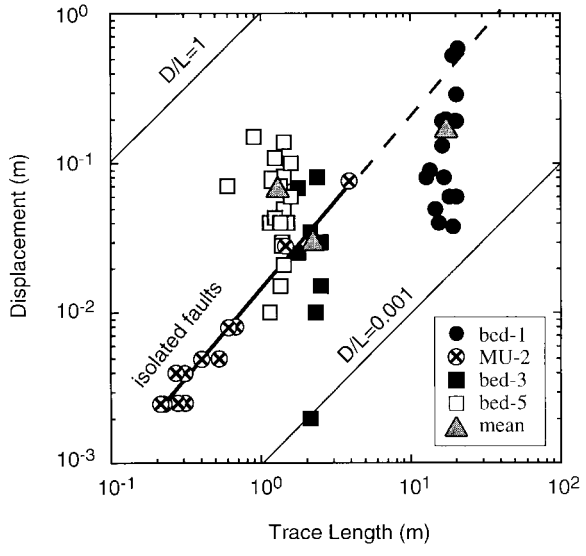

Fig. 9. Plot of maximum displacement (D) versus cross-sectional trace length (L) for Set 1 faulted joints in Beds 1, 3, and 5 and for isolated primary faults in Mechanical Unit 2 (MU 2). Note that D is independent of L for faulted joints, although all data fall within the range of D/L ratios (0.001–1) reported in cumulative global datasets.

Upon restoration of bedding to horizontal the Set 1 joints become subvertical (Fig. 8a). The mean pole to rotated Set 1 joints plunges 09° to 206°, suggesting to us that σ_3 was subhorizontal and aligned NNE–SSW during Set 1 joint development. Principal stresses can be derived from primary conjugate faults using a simple geometric analysis where the σ_1 axis bisects the obtuse angle between the two fault sets, the σ_2 axis corresponds to the line of intersection of the two fault sets, and the σ_3 axis bisects the acute angle between the faults (Anderson, 1951; Angelier, 1994). Geometric stress analyses applied to conjugate fault sets have been validated by field studies (e.g. Angelier, 1979a; Eyal and Reches, 1983; Gross, 1995). The subvertical and shallow-dipping in situ inclinations for the two primary fault sets (Fig. 4e) are strikingly similar to conjugate fault sets reported by Angelier et al. (1985) and Angelier (1989) that formed prior to tilting. We therefore calculated principal stresses using the rotated mean conjugate fault orientations upon restoration of bedding to horizontal. Results show a subvertical maximum principal stress (σ_1) and a subhorizontal least principal stress (σ_3) that is closely aligned with the mean pole to Set 2 joints and the mean rotated pole to Set 1 joints (Fig. 8a). Relative timing relations between Set 1 joints and primary faults could not be determined because the two structural elements are restricted to different beds. However, the similarity in calculated principal stress axes suggests to us that Set 1 joints and primary faults may have formed coevally in different lithological units during an early phase of deformation. Fracture partitioning, the process whereby joints and faults developed in different lithological units in response to the same applied remote stress, is commonly observed in layered rocks characterized by high competency contrasts (Gross, 1995).

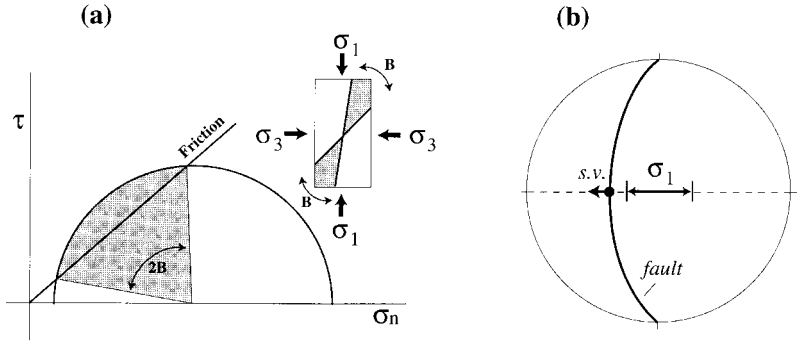

Fig. 10. Frictional sliding envelope (A) and stereoplot (B) showing the wide range in possible orientations of σ_1 axis with respect to a faulted joint.

3.7. Kinematic and stress analysis of faulted joints

The spatial association of pinnate joints with sheared Set 1 joints, the parallelism of Set 2 joints with pinnate joints, and dip-slip striations on sheared Set 1 joints consistent with principal stress axes during Set 2 joint development, all suggest a kinematic coherence among these structural elements. Our goal is to constrain the stress conditions that led to slip along Set 1 joints. An assumption inherent to most stress analyses applied to fault populations is that the stress tensor is uniform over the region of study for a given phase of deformation (Gephart and Forsyth, 1984; Angelier, 1994). Stress inversion analysis, a methodology developed over the past 20 years, has been successfully applied to populations of striated faults (e.g. Carey and Brunier, 1974; Angelier 1979a,b; Etchecopar et al., 1981; Reches, 1987). Stress inversion utilizes fault slip data to quantitatively solve for the best-fit principal stress tensor by minimizing the misfit angle between the observed and predicted slip directions on a fault plane (Angelier, 1994). Stress inversion is ideally suited for large data sets consisting of a variety of fault orientations and slip vectors; however, it is not effective for a single population of uniformly oriented faults and slip vectors (Angelier, 1994). This ineffectiveness is because frictional sliding across a pre-existing fracture can occur in response to a wide range of principal stress orientations relative to the fracture plane (Fig. 10), and faults of other orientations are required to reduce the possible choices of the stress axes. Therefore, an alternative method must be employed to establish the kinematics of faulted joints observed at this outcrop.

Our first assumption is that pinnate joints and slip along Set 1 joints occur during the same phase of deformation. This assumption is based on the observations that (1) pinnate joint development is closely associated with slipped Set 1 joints, and (2) pinnate joints are restricted to the dilational quadrants in the hanging walls and footwalls of faulted joints. Because pinnate joints are opening-mode fractures, the least principal stress, σ_3, during this phase of deformation likely corresponds to the pole to the mean pinnate joint plane (Fig. 8b). Although σ_1 and σ_2 must fall within the pinnate joint plane, their trends and plunges can only be constrained with additional information. That information is provided by the mean slip vector along faulted Set 1 joints. For pure dip slip motion, the maximum compressive stress axis (σ_1) falls within the plane that contains both the slip vector and the normal to the fault plane (Angelier, 1994). Therefore, σ_1 must lie at the intersection between the mean pinnate joint plane and the plane that is normal to the mean faulted joints (Fig. 8b). The intermediate principal stress axis is then easily solved for as the line mutually perpendicular to the other two stress axes.

Set 2 joints, pinnate joints, and wing cracks are aligned parallel to one another. Although formation of these fractures relative to one another is not constrained by abutting relations, all of these fracture sets display consistent terminations against Set 1 joints. Furthermore, their subvertical alignment and lack of slip suggests they may have developed after tilting of the strata (e.g. Hancock and Engelder, 1989). Upon rotation of bedding to horizontal, the mean pole of Set 1 joints falls within the 95% confidence cone of the mean pole of Set 2 joints (and therefore pinnate joints too; Fig. 8a). Furthermore, principal stress axes derived from the pinnate joints and faulted joints (Fig. 8b) are nearly identical to the principal stress axes derived from the restored primary faults and Set 1 joints (Fig. 8a). This correspondence suggests to us that principal stress axes may have remained uniformly oriented throughout fracture development. The rotation of pre-existing Set 1 joints as a result of tilting of bedding within a fixed principal stress configuration would lead to a resolved shear traction across Set 1 joints, and hence may have enhanced the possibility of slip along these planes of weakness (Fig. 11).

4. Discussion

4.1. Distinguishing characteristics of pinnate joints

The observed field relations provide important distinctions between pinnate joints and other types of "secondary" (Cruikshank et al., 1991; Martel, 1997) or "splay" fractures

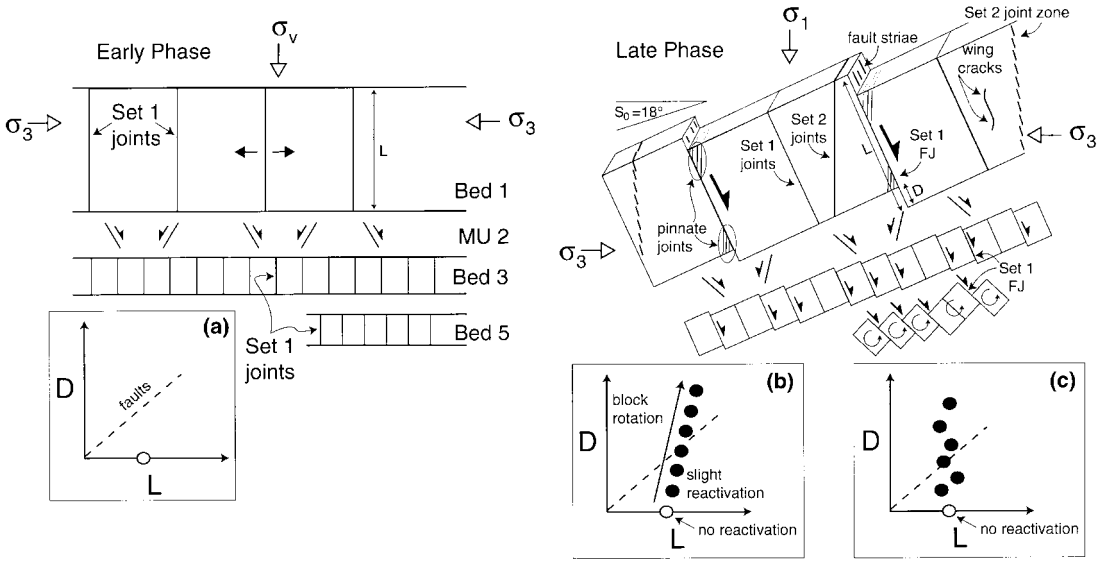

Fig. 11. Schematic model (not to scale) depicting structural evolution of fractures at outcrop. Set 1 joints formed in jointed Beds 1, 3, and 5 during early phase (horizontal strata), possibly concurrent with primary faulting in shale beds (MU 2). Set 2 joints, pinnate joints, and faulting of Set 1 joints occurred later in jointed beds as the strata were tilted. Schematic *D–L* graphs (arithmetic scale) depict a joint of finite length but no shear offset (A) and the projected path for a single faulted joint as slip accumulates through time (B). (C) Expected *D–L* for a population of faulted joints, due to differences in initial lengths prior to reactivation.

(Martel and Pollard, 1989; Cooke, 1997). Laboratory experiments and numerical models predict that the orientation of splay fractures emanating from fault tips will vary (a) due to local stress perturbations near the fault tip that would result in curved fractures (Nemat-Nasser and Horii, 1982), (b) as a function of the ratio of shear stress responsible for kinking to the normal stress associated with joint opening (Cotterell and Rice, 1980; Cruikshank et al., 1991), (c) in response to variations in fault-parallel normal stress (Willemse and Pollard, 1998), and (d) as a function of frictional strength along the fault (Cooke, 1997). The clustering of pinnate joints in dilational quadrants is consistent with the general localization of secondary extension fractures caused by a slip-induced increase in tensile stress. However, the parallelism of pinnate joints to the Set 2 subvertical joints (Fig. 4c, d), as well as their strong planarity (lack of curvature), implies that pinnate joint orientation is controlled by the orientations of remote principal stresses rather than by a localized reorientation of the stress field in the vicinity of fault tips. In addition, the pinnate joints at Split Mountain did not initiate from fault tips, as is the case for wing cracks (Willemse and Pollard, 1998) or kinks (Cruikshank et al., 1991). The lack of deformation at the tip of a propagating fault is known because the host fractures are bed-confined reactivated joints with tips at bed boundaries prior to faulting and development of the secondary pinnate joints (Fig. 5). The presence of pinnate joints branching from both unfaulted joints as well as faulted joints suggests to us that some pinnate joints develop prior to fault slip rather than as a direct consequence of fault slip. The cause for this pre-slip development could be pre-fault stress accumulation in the wall rock, thus suggesting that pinnate joints may also serve as precursors to slip.

Structural geometries and timing relations of fractures documented in this study further support the conclusions of Hancock (1985) and Engelder (1989) that pinnate joints may serve as effective kinematic indicators. The observed ~20° mean angle between pinnate joints and host faults at this outcrop is considerably less than the conventional 30–35° angle between σ_1 and isolated primary fault planes predicted by Coulomb fracture criterion. As noted by Angelier (1994), a meaningful stress inversion analysis of reactivated fractures requires a wide range of fault orientations that slipped during the same phase of deformation. Thus, in outcrops or regions characterized by populations of uniformly oriented faults, pinnate joints may help to constrain paleostress axes, especially if they formed coevally with a systematic joint set (e.g. Set 2 in this study).

4.2. Scaling of faulted joints and its implications

Compilations of fault data in the literature portray a general correlation between length and displacement (i.e. scale independence), which in turn fits nicely with some current models for fault growth (e.g. Cowie and Scholz, 1992a). However, global compilations of faults at different scales tend to mask significant differences among data sets, and thus may lead to the false impression of a correlation (Cowie and Scholz, 1992b; Clark and Cox, 1996; Gross et al., 1997). For example, *D*/*L* ratios for faulted joints at Split Mountain fall within the broad range of 0.001–1.0 prescribed for scale-independent faults (Cowie and Scholz, 1992b; Schlische et al., 1996), yet these faults do not exhibit

scale independence (Fig. 9). If the initial geometries, origin, and development of faulted joints are fundamentally different from isolated primary faults, then one could expect different *D*–*L* relations.

Faulted joints at Split Mountain have approximately the same cross-sectional trace length within a given bed (Fig. 9). This trace length distribution is expected if the faults originated as joints confined to competent beds (e.g. Narr and Suppe, 1991; Gross et al., 1995) with upper and lower tips at bed boundaries (Fig. 5). Thus, on an arithmetic scale, an unfaulted joint will plot as a fracture with finite trace length (proportional to mechanical bed thickness) but zero shear displacement (Fig. 11). Once slip begins, progressive shearing of individual faulted joints produces a steep path on *D*–*L* plots because the length increase due to incremental slip is small relative to the initial joint length. A group of joints subjected to minor amounts of reactivation (e.g. Bed 1 faulted joints) would plot below the "predicted" *D*/*L* line for scale-invariant isolated primary faults, whereas faulted joints that accommodate block rotation (e.g. Bed 5) would plot above this line due to greater slips (Figs. 9 and 11b). This interpretation explains why the average *D*/*L* values for Bed 5 are relatively greater than those for Beds 1 and 3 (Fig. 9).

The lack of correlation between displacement and length is a logical consequence of the faults attaining most of their length prior to slip, in contrast to primary faults that incrementally accrue slip as they propagate. Displacement magnitudes due to shear reactivation should depend upon local stress and strain conditions for each joint rather than a universal fault growth model, leading to a wide range of displacements for faults within a given bed (Fig. 11c). Lateral variations in bed thickness would result in differences in initial joint length within each bed, which may be greater than the differences in shear displacement, further contributing to a population of faults whose displacement is independent of length. However, as the faulted joints accommodate larger amounts of strain, renewed propagation will occur which may adhere to scale-independent fault growth.

Faults that originated as joints must be correctly identified and treated separately from isolated primary faults in terms of kinematics and displacement–length analysis. One cannot infer or predict a displacement or gouge thickness based solely on inputting fault length into a universal scaling law, because (1) displacement across a faulted joint may be unrelated to its length and (2) growth of the initial joint did not generate fault gouge. Consequently, in the absence of structural constraints (e.g. geometric and kinematic data), assuming fault zone sizes and permeabilities from limited data sets (i.e. borehole, core, seismic, poor outcrop exposure) may lead to erroneous conclusions regarding strain estimates, slip estimates, and subsurface fluid flow, especially if the latter is related to fault length and/or fault zone width.

The large scatter in published *D*–*L* plots, especially at the mesoscale, may in part reflect the presence of faulted joints among the measured faults. Walsh and Watterson (1988) and Cowie and Scholz (1992b) recognized that mechanical properties influence *D*/*L* ratios, and therefore concluded that scaling of *D* with *L* should occur only for populations of faults within similar lithologies (i.e. mechanical properties). Wojtal (1994, 1996) showed that frequency–size scaling relations for faults may change due to restrictive effects of bed boundaries, segment linkage, and duplex formation. Cartwright et al. (1995) identified along-strike segment linkage as a factor contributing to scatter in *D*–*L* plots. Gross et al. (1997) reported a complete breakdown in *D*–*L* scaling for normal faults due to effects of mechanical stratigraphy and changes in kinematics. This study demonstrates that faults at the same outcrop and found within the same rock type do not initially adhere to a linear scaling between *D* and *L* if they originated as faulted joints.

4.3. Selection of length dimension for D–L analysis

Many recent studies of normal faults have documented variations in displacement along strike, often by measuring the scarp height separating a single offset marker horizon (e.g. Dawers et al., 1993; Cartwright et al., 1995; Schlische et al., 1996). This method provides superior displacement profiles because a nearly continuous stream of data can be collected, and raises the issue of whether the lack of scaling for faulted joints reported in our study is simply a function of measuring length in cross-section (i.e. down dip) rather than along strike. However, analysis of the fault-scaling literature and the data presented in this study prove otherwise. First, *D*–*L* scaling relations have been established for normal faults in both cross-section (e.g. Muraoka and Kamata, 1983) and plan view (e.g. Dawers et al., 1993). Second, the conclusion that *D*–*L* is scale invariant is partially based on faults measured in cross-section and/or fault length defined as the dimension parallel to the slip vector. Without exception, all "global data set" compilations used for establishing scale invariance (e.g. Walsh and Watterson, 1988; Marrett and Allmendinger, 1991; Peacock, 1991; Cowie and Scholz 1992a,b; Gillespie et al., 1992; Cartwright et al., 1995; Schlische et al., 1996) consist of a combination of fault data measured in plan view and cross-section, as well as a variety of fault types (e.g. strike slip, normal, thrust, oblique), such that the length dimension is often parallel to the slip vector. Third, along-strike measurements of normal fault scarps are limited to a single offset horizon that does not necessarily represent the largest separation. Hence, they are less likely to yield maximum fault displacement when compared to cross-sectional surveys, especially for faults that initiate beneath the earth's surface. Fourth, and most importantly, in the data set that we provide, *D*–*L* scales linearly for primary faults, but not for the faulted joints within the same outcrop. Both types of faults were measured in cross-section, and two of the three groups of faulted joints fall within the length range

of primary faults (Fig. 9). Therefore, the lack of scaling for faulted joints is not a function of the measurement method or data collection from different locations, but rather due to the inherent genetic differences between the two types of faults.

4.4. Criteria for identifying faulted joints

Several criteria may be employed to distinguish faulted joints from primary faults. One important clue is whether the faulted joints belong to a larger set of parallel fractures that include pure opening-mode joints, which might imply an opening-mode origin for all fractures of that set (Segall and Pollard, 1983). This interpretation can be further verified by the presence of plumes on unfaulted joints, as well as by partially erased plumes on faulted joints. Non-Coulomb behavior provides circumstantial evidence, because primary faults often appear as conjugate pairs forming acute angles of ~60°. Faults with different orientations but sharing the same slip vector also indicate reactivation, but do not necessarily imply a jointing origin for all fractures (Angelier, 1994). This study provides additional criteria for identifying faulted joints: the absence of fault breccia or gouge for faults of considerable length (e.g. 12 + m faulted joints in Bed 1 without gouge/breccia), spacing distributions similar to confined joint sets in layered sedimentary rocks (Fig. 6), subperpendicular alignment with bedding (Figs. 2 and 4), termination of faults at bed boundaries (Fig. 5), and, most significantly, fault displacements that are independent of length (Fig. 9).

5. Summary

Geometries and kinematics of brittle deformation features found within the Chinle Formation and Glen Canyon Sandstone at Split Mountain, Utah, reveal that early subvertical joints confined to jointed beds were subsequently reactivated in shear. Reactivation of the joints with normal dip-slip produced "faulted joints", which are interpreted to have formed in conjunction with a second set of joints and clusters of pinnate joints. Faulted joints in layered rocks may be identified by their geometric similarities to non-faulted, bed-confined joints: their positively skewed spacing distributions, their lack of conjugate pairs, their consistent terminations at or near discrete bed boundaries, and the absence of significant amounts of fault breccia and/or gouge. Because faulted joints attain considerable length prior to slip, their D/L ratios are initially much smaller than those for primary faults. Furthermore, magnitude of slip is not a consequence of fault growth, and consequently displacement across faulted joints in certain cases may be independent of length. This study emphasizes the need to evaluate the origin, kinematics, geometries, and mechanisms of fault development as they relate to fault scaling attributes.

Acknowledgements

Funding for this project was provided by the United States–Israel Binational Science Foundation Grant No. 94-00396. We dedicate this paper to the memory of Paul Hancock, who pioneered the use of pinnate joints as kinematic indicators. We benefited from discussions in the field with Laura Silliphant and Dave McConaughy. Excellent reviews by Juliet Crider, Randall Marrett, William Dunne, Juan Watterson, and an anonymous reviewer are gratefully appreciated.

References

Anderson, E.M., 1951. The Dynamics of Faulting and Dyke Formation with Applications to Britain. Oliver & Boyd, Edinburgh.

Angelier, J., 1979a. Neotectonique de L'Arc Egeen. Societe Geologique du Nord 3, 418.

Angelier, J., 1979b. Determination of the mean principal directions of stresses for a given fault population. Tectonophysics 56, 17–26.

Angelier, J., 1989. From orientation to magnitudes in paleostress determinations using fault slip data. Journal of Structural Geology 11, 37–50.

Angelier, J., 1994. Fault slip analysis and paleostress reconstruction. In: Hancock, P.L. (Ed.), Continental Deformation. Pergamon Press, Oxford, pp. 53–100.

Angelier, J., Colletata, B., Anderson, R.E., 1985. Neogene paleostress changes in the Basin and Range: a case study at Hoover Dam, Nevada–Arizona. Geological Society of America Bulletin 96, 347–361.

Bahat, D., 1988. Early single-layer and late multi-layer joints in the Lower Eocene chalks near Beer Sheva, Israel. Annales Tectonicae 2, 3–11.

Bates, R.L., Jackson, J.A. (Eds.), 1995. Dictionary of Geological Terms, 3rd ed. American Geological Institute, New York.

Beach, A., 1975. The geometry of en-echelon vein arrays. Tectonophysics 28, 245–263.

Becker, A., Gross, M.R., 1996. Mechanism for joint saturation in mechanically layered rocks: an example from southern Israel. Tectonophysics 257, 223–237.

Caine, J.S., Evans, J.P., Forster, C.B., 1996. Fault zone architecture and permeability structure. Geology 24, 1025–1028.

Carey, E., Brunier, B., 1974. Analyse theorique et numerique d'un modele mecanique elementaire applique a l'etude d'une population de failles. Comptes Rendues Academie de Science de Paris 279, 891–894.

Cartwright, J.A., Trudgill, B.D., Mansfield, C.S., 1995. Fault growth by segment linkage: an explanation for scatter in maximum displacement and trace length data from the Canyonlands Grabens of SE Utah. Journal of Structural Geology 17, 1319–1326.

Childs, C., Walsh, J.J., Watterson, J., 1990. A method for estimation of the density of fault displacements below the limit of seismic resolution in reservoir formations. In: Buller, A.T., Berg, E., Hjelmeland, O., Kleppe, J., Torsaeter, O., Aasen, J.O. (Eds.), North Sea Oil and Gas Reservoirs II. Graham & Trotman, London, pp. 309–318.

Clark, R.M., Cox, S.J.D., 1996. A modern regression approach to determining fault displacement–length scaling relationships. Journal of Structural Geology 18, 147–152.

Cooke, M.L., 1997. Fracture localization along faults with spatially varying friction. Journal of Geophysical Research 102, 22,425–22,434.

Cotterell, B., Rice, J.R., 1980. Slightly curved or kinked cracks. International Journal of Fracture 16, 155–169.

Cowie, P.A., Scholz, C.H., 1992a. Physical explanation for the displacement–length relationship of faults using a post-yield fracture mechanics model. Journal of Structural Geology 14, 1133–1148.

Cowie, P.A., Scholz, C.H., 1992b. Displacement–length scaling

relationships for faults: data synthesis and discussion. Journal of Structural Geology 14, 1149–1156.
Cruikshank, K.M., Zhao, G., Johnson, A.M., 1991. Analysis of minor fractures associated with joints and faulted joints. Journal of Structural Geology 13, 865–886.
Dawers, N.H., Anders, M.H., 1995. Displacement–length scaling and fault linkage. Journal of Structural Geology 17, 607–614.
Dawers, N.H., Anders, M.H., Scholz, C.H., 1993. Growth of normal faults: displacement–length scaling. Geology 21, 1107–1110.
Engelder, T., 1989. Analysis of pinnate joints in the Mount Desert Island granite: implications for post-intrusion kinematics in the coastal volcanic belt, Maine. Geology 17, 564–567.
Engelder, T., Logan, J.M., Handin, J., 1975. The sliding characteristics of sandstone on quartz fault-gouge. Pure and Applied Geophysics 113, 69–86.
Etchecopar, A., Vasseur, G., Daignieres, M., 1981. An inverse problem in microtectonics for the determination of stress tensors from fault striation analysis. Journal of Structural Geology 3, 51–65.
Evans, J.P., Forster, C.B., Goddard, J.V., 1997. Permeability of fault-related rocks, and implications for hydraulic structure of fault zones. Journal of Structural Geology 19, 1393–1404.
Eyal, Y., Reches, Z., 1983. Tectonic analysis of the Dead Sea rift region since the Late-Cretaceous based on mesostructures. Tectonics 2, 167–185.
Gephart, J.W., Forsyth, D., 1984. An improved method for determining the regional stress tensor using earthquake focal plane mechanism data: application to the San Fernando earthquake sequence. Journal of Geophysical Research 89, 9305–9320.
Gillespie, P.A., Walsh, J.J., Watterson, J., 1992. Limitations of dimension and displacement data from single faults and the consequences for data analysis and interpretation. Journal of Structural Geology 14, 1157–1172.
Gross, M.R., 1993. The origin and spacing of cross joints: examples from the Monterey Formation, Santa Barbara coastline, California. Journal of Structural Geology 15, 737–751.
Gross, M.R., 1995. Fracture partitioning: failure mode as a function of lithology in the Monterey Formation of coastal California. Geological Society of America Bulletin 107, 779–792.
Gross, M.R., Fischer, M.P., Engelder, T., Greenfield, R.J., 1995. Factors controlling joint spacing in interbedded sedimentary rocks: integrating numerical models with field observations from the Monterey Formation, USA. In: Ameen, M.S. (Ed.), Fractography: Fracture Topography as a Tool in Fracture Mechanics and Stress Analysis. Geological Society Special Publication No. 92, Geological Society, pp. 215–233.
Gross, M.R., Gutiérrez-Alonso, G., Bai, T., Wacker, M.A., Collinsworth, K.B., Behl, R.J., 1997. Influence of mechanical stratigraphy and kinematics on fault scaling relations. Journal of Structural Geology 19, 171–183.
Hancock, P.L., 1972. The analysis of en-echelon veins. Geological Magazine 109, 269–276.
Hancock, P.L., 1985. Brittle microtectonics: principles and practice. Journal of Structural Geology 7, 437–457.
Hancock, P.L., Engelder, T., 1989. Neotectonic joints. Geological Society of America Bulletin 101, 1197–1208.
Hansen, W.R., 1986. History of faulting in the eastern Uinta Mountains, Colorado and Utah. In: Stone, D.S., Johnson, K.S. (Eds.), New Interpretations of Northwest Colorado Geology. Rocky Mountain Association of Geologists—1986 Symposium, pp. 5–17.
Helgeson, D., Aydin, A., 1991. Characteristics of joint propagation across layer interfaces in sedimentary rocks. Journal of Structural Geology 13, 897–911.
Ji, S., Saruwatari, K., 1998. A revised model for the relationship between joint spacing and layer thickness. Journal of Structural Geology 20, 1495–1508.
Lockner, D.A., Byerlee, J.D., Kuksenko, V., Ponomarev, A., Sidorin, A., 1992. Observations of quasistatic fault growth from acoustic emissions. In: Evans, B., Wong, T.F. (Eds.), Fault Mechanics and Transport Properties of Rocks. Academic Press, San Diego, pp. 3–31.
Marone, C., Scholz, C.H., 1989. Particle-size distribution and microstructures within simulated fault gouge. Journal of Structural Geology 11, 799–814.
Marrett, R., Allmendinger, R.W., 1991. Estimates of strain due to brittle faulting: sampling of fault populations. Journal of Structural Geology 13, 735–738.
Marrett, R., Allmendinger, R.W., 1992. Amount of extension on "small" faults: an example from the Viking graben. Geology 20, 47–50.
Martel, S.J., 1997. Effects of cohesive zones on small faults and implications for secondary fracturing and fault trace geometry. Journal of Structural Geology 19, 835–847.
Martel, S.J., Pollard, D.D., 1989. Mechanics of slip and fracture along small faults and simple strike-slip fault zones in granitic rock. Journal of Geophysical Research 94, 9417–9428.
Mollema, P.N., Antonellini, M., 1999. Development of strike-slip faults in the dolomites of the Sella Group, Northern Italy. Journal of Structural Geology 21, 273–292.
Muraoka, H., Kamata, H., 1983. Displacement distribution along minor fault traces. Journal of Structural Geology 5, 483–495.
Narr, W., Suppe, J., 1991. Joint spacing in sedimentary rocks. Journal of Structural Geology 13, 1037–1048.
Nemat-Nasser, S., Horii, H., 1982. Compression-induced nonplanar crack extension with application to splitting, exfoliation, and rockburst. Journal of Geophysical Research 87, 6805–6821.
Opheim, J.A., Gudmundsson, A., 1989. Formation and geometry of fractures, and related volcanism, of the Krafla fissure swarm, northeast Iceland. Geological Society of America Bulletin 101, 1608–1622.
Peacock, D.C.P., 1991. Displacement and segment linkage in strike-slip fault zones. Journal of Structural Geology 13, 1025–1035.
Peacock, D.C.P., Sanderson, D.J., 1991. Displacements, segment linkage and relay ramps in normal fault zones. Journal of Structural Geology 13, 721–733.
Ramsay, J.G., Huber, M.I., 1987. The Techniques of Modern Structural Geology, Vol. 2: Folds and Fractures. Academic Press, London.
Reches, Z., 1987. Determination of the tectonic stress tensor from slip along faults that obey the Coulomb yield criterion. Tectonics 6, 849–861.
Rowley, P.D., Hansen, W.R., 1979. Geologic Map of the Split Monument Quadrangle, Uinta County, Utah. US Geological Survey Map GQ-1515, scale 1:24,000.
Ruf, J.C., Rust, K.A., Engelder, T., 1998. Investigating the effect of mechanical discontinuities on joint spacing. Tectonophysics 295, 245–257.
Schlische, R.W., Young, S.S., Ackermann, R.V., Gupta, A., 1996. Geometry and scaling relations of a population of very small rift-related normal faults. Geology 24, 683–686.
Scholz, C.H., 1968. Experimental study of the fracturing process in brittle rock. Journal of Geophysical Research 73, 1447–1454.
Segall, P., Pollard, D.D., 1983. Nucleation and growth of strike slip faults in granite. Journal of Geophysical Research 88, 555–568.
Silliphant, L.J., 1998. Regional and fold-parallel joint distribution at Split Mountain, Utah: a study of the relationship between joint development and 2-D curvature in Laramide folds. M.S. thesis, The Pennsylvania State University.
Walsh, J.J., Watterson, J., 1988. Analysis of the relationship between displacements and dimensions of faults. Journal of Structural Geology 10, 239–247.
Watterson, J., 1986. Fault dimensions, displacements, and growth. Pure and Applied Geophysics 24, 365–373.
Wilkins, S.J., 1999. The influence of mechanical layering on the evolution of brittle structures: fracture partitioning and fault growth. M.S. thesis, Florida International University.
Willemse, E.J.M., 1997. Segmented normal faults: correspondence between three-dimensional mechanical models and field data. Journal of Geophysical Research 102, 675–692.
Willemse, E.J.M., Peacock, D.C.P., Aydin, A., 1997. Nucleation and

growth of strike-slip faults in limestones from Somerset, UK. Journal of Structural Geology 19, 1461–1477.

Willemse, E.J.M., Pollard, D.D., 1998. On the orientation and patterns of wing cracks and solution surfaces at the tips of a sliding flaw or fault. Journal of Geophysical Research 103, 2427–2438.

Wojtal, S.F., 1994. Fault scaling laws and the temporal evolution of fault systems. Journal of Structural Geology 16, 603–612.

Wojtal, S.F., 1996. Changes in fault displacement populations correlated to linkage between faults. Journal of Structural Geology 18, 265–279.

Younes, A.I., Engelder, T., 1999. Fringe cracks: key structures for the interpretation of the progressive Alleghanian deformation of the Appalachian plateau. Geological Society of America Bulletin 111, 219–239.

Zhang, S., Tullis, T., 1998. The effect of fault slip on permeability and permeability anisotropy in quartz gouge. Tectonophysics 295, 41–52.